

Received 14 October 2022, accepted 2 November 2022, date of publication 10 November 2022, date of current version 16 November 2022.

Digital Object Identifier 10.1109/ACCESS.2022.3221456

## RESEARCH ARTICLE

# Identification of PPG Measurement Sites Toward Countermeasures Against Biometric Presentation Attacks

SHUN HINATSU<sup>1,2</sup>, NORI MATSUDA<sup>1</sup>, HIROKI ISHIZUKA<sup>1,2</sup>,  
SEI IKEDA<sup>1,2</sup>, (Member, IEEE), AND OSAMU OSHIRO<sup>1,2</sup>

<sup>1</sup>Information Technology Research and Development Center, Mitsubishi Electric Corporation, Kamakura 247-8501, Japan

<sup>2</sup>Graduate School of Engineering Science, Osaka University, Toyonaka 560-8531, Japan

Corresponding author: Shun Hinatsu (Hinatsu.Shun@bc.MitsubishiElectric.co.jp)

This work involved human subjects or animals in its research. Approval of all ethical and experimental procedures and protocols was granted by the Ethical Committee of Information Technology Research and Development Center, Mitsubishi Electric Corporation under Application No. 2020-B001.

**ABSTRACT** In this study, we propose a countermeasure against a presentation attack on a photoplethysmogram (PPG)-based biometric authentication system. The countermeasure detects fake PPG signals by identifying PPG measurement sites on the body based on the difference between PPG waveforms recorded at genuine measurement and non-genuine sites without adding other sensing components. In an experiment, we computed the correlation coefficients as the similarity indices between PPG waveforms using two datasets, i.e., PPG signals recorded at multiple measurement sites on participants and mapped signals to generate fake signals for authentication. We then evaluated the proposed countermeasure using the feature values extracted from the PPG signals to identify the measurement sites on the body. The experimental results indicated that the identification of measurement sites as a countermeasure operated successfully for both PPG datasets, regardless of the presence or absence of waveform mapping, and exhibited an identification accuracy of more than 90 % regardless of the elapsed time.

**INDEX TERMS** Biometrics, measurement site, photoplethysmogram, and waveform mapping.

## I. INTRODUCTION

Blood circulation through our bodies, driven by the heart, contains several physiological pieces of information. For example, the contraction and expansion of blood vessels during circulation reflect cardiac activities such as heartbeat and heart rate variability [1]. Electrocardiogram (ECG) measurements are frequently used to observe these cardiac activities [2], while photoplethysmogram (PPG) measurements can also be used based on blood circulation [3]. PPG measurement is an optical technique that uses a sensor comprising a light source such as a light emitting diodes (LED) and a photodetector such as a phototransistor (PTr), or camera to detect blood volume changes [3]. The measurement has fewer restrictions than the ECG measurement because it requires

only one sensor on various measurement sites on the body, whereas ECG measurement requires multiple electrodes on the body. Commercially available wearable devices, such as smartwatches, provide PPG measurement functions by utilizing the characteristics of PPG measurements. These functions can be used for healthcare applications such as the estimation of heart rate [4]. In addition, several approaches have been proposed to apply PPG signals to biometric authentication by utilizing the personal distinctiveness of waveforms [5], [6]. PPG-based authentication is expected to seamlessly connect applications and authentication functions using one PPG sensor [7].

However, several studies have also been conducted on identity spoofing in biometric systems using physiological signals such as time-series PPG signals [8], [9], [10]. During spoofing, an attacker impersonates a genuine person (victim) by generating and presenting fake signals to the system.

The associate editor coordinating the review of this manuscript and approving it for publication was Kin Fong Lei<sup>1</sup>.

In general, a PPG waveform is recorded at various measurement sites on the body [11], [12], and reconstructed by using only a few frequency components [13], which may contribute to the generation of fake PPG signals. In addition, artificial PPG signals can be generated using several techniques, such as an optical approach to modulate the light intensity and a physical approach to compress the upper arm as the measurement site [14], [15]. Attackers can easily generate fake PPG signals to break the PPG-based authentication based on waveform characteristics and signal-generation techniques. Therefore, methods to detect fake PPG signals and PPG-based authentication with countermeasures against identity spoofing must be developed.

In this paper, we propose a countermeasure against identity spoofing on PPG-based authentication. We focus on existing spoofing of PPG-based authentication derived from the leakage of information required for authentication by PPG recording at non-genuine measurement sites, and the variability of PPG waveforms recorded at different sites on the body. The proposed countermeasure identifies PPG measurement sites by comparing the waveforms to detect fake PPG signals without adding other sensing components. We evaluated the countermeasures in an experiment using PPG signal datasets recorded at multiple measurement sites on the body.

## II. RELATED STUDIES

### A. ATTACKS ON PHYSIOLOGICAL SIGNAL-BASED BIOMETRIC AUTHENTICATION

Many studies have been conducted on identity spoofing in physiological signal-based biometric authentication, while many biometric authentication approaches are available. Several studies have investigated presentation attacks (PA) that present fake biometrics to a sensor in a biometric authentication system [8], [9]. Many PAs are derived from information leakage: the information required for authentication is obtained by an attacker in non-genuine ways. Eberz et al. investigated a PA on ECG-based authentication that was conducted using a commercially available wearable authentication device on a user's wrist. The PA maps ECG signals recorded at non-genuine measurement sites to generate fake signals transmitted to a device [8]. Shukla et al. investigated a PA on electroencephalogram (EEG)-based authentication that was conducted using multiple electrodes on the user's head. The PA estimated the original EEG waveforms by utilizing the correlation between the EEG signals recorded by the electrodes and the accelerometer data derived from the victim's movements during the EEG recording [9]. In addition, as shown in Fig. 1, several studies have warned PAs may be performed on PPG-based biometric authentication using various PPG measurement sites on a victim's body and generating fake PPG signals to inject into the smartwatch as the authentication device [10], [16]. Seepers et al. investigated a PA on PPG-based authentication using heartbeats estimated based on PPG recorded at the face using a camera [10]. Our previous study also investigated

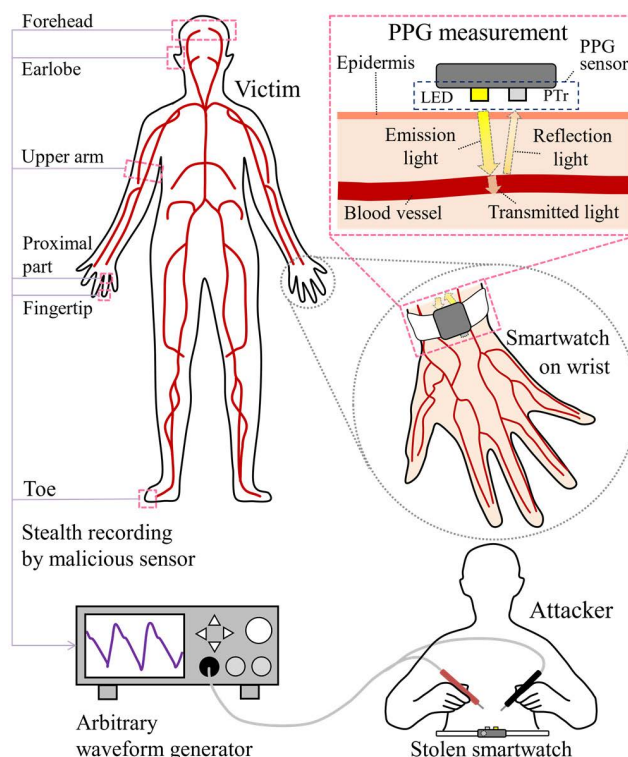


**FIGURE 1.** Abstract of PPG measurement and PA against PPG-based authentication.

a PA on PPG-based authentication utilizing PPG signals recorded at non-genuine measurement sites on a body by installing malicious PPG sensors [17]. We also investigated a PPG waveform mapping method to generate fake signals based on frequency characteristics to improve PA [18]. In addition, Li et al. proposed a waveform mapping method using PPG signals recorded at the face and a generative adversarial network (GAN) for a PA on PPG-based authentication [16]. Therefore, countermeasures are required against PAs by using waveform mapping techniques for PPG-based authentication.

### B. COUNTERMEASURES AGAINST PAs

Some of the most general countermeasures against PAs are liveness detection methods [19], which ascertain that the input is an actual measurement from the authorized, alive person who is present at the time of measurement [20]. Liveness detection methods are classified into static, dynamic, behavioral, and biometric quality-based techniques [21]. Physiological signals, such as PPG signals are often used for static liveness detection in face recognition systems [22]. Meanwhile, PPG waveforms as biometric quality depend not only on individuals but also on measurement sites [11], [23]. PAs against PPG-based authentication are based on the leakage of the information required for authentication derived from PPG signals recorded at impostor measurement sites [16], [18]. Therefore, if liveness detection can be performed using one

PPG signal as a biometric quality-based technique without adding other sensing components, it may connect PPG-based authentication and the countermeasure against the PA with one PPG sensor [7].

Continuous authentication can also be used as a countermeasure against identity spoofing, such as PAs on biometric authentication systems, which repeats the identification of genuine or impostor after an initial authentication [24]. Generally, continuous authentication systems require soft biometrics, which are non-intrusive, behavioral, or material accessories such as face and clothing colors associated with an individual [25], whereas hard biometrics include unique and permanent personal characteristics such as fingerprint and iris texture [26], [27]. However, soft biometrics, such as face and clothing colors, cannot frequently be used for individual authentication alone [24]. PPG signals include biometric information that can be used as both hard and soft biometrics [28]. Several studies used soft biometrics extracted from PPG signals, such as their periodicity recorded by a camera for continuous authentication against PAs on face recognition systems [29]. Therefore, if wearable devices can provide both initial and continuous authentication using one PPG sensor, they may connect several applications, such as healthcare monitoring, with the initial authentication, liveness detection and continuous authentication seamlessly.

Meanwhile, in addition to liveness detection and continuous authentication, several studies have focused on the relationships between physiological signal waveform quality and measurement sites [11], [23]. For example, Hartmann et al. conducted a quantitative comparison of PPG waveforms and feature values extracted from waveforms at multiple measurement sites on a body [11]. To obtain high-quality PPG waveforms, Reddy et al. proposed a detection method for PPG sensor disconnections from a specific measurement site on a body, focusing on the saturation of signal waveforms [30]. However, research on the identification of PPG measurement sites using PPG waveforms as a countermeasure against PAs without adding other components is lacking. The relationships between PPG waveforms and measurement sites may contribute to countermeasures against PAs derived from information leakages on non-genuine sites.

### III. PROPOSED COUNTERMEASURE

We propose a countermeasure against PAs for PPG-based authentication using PPG waveforms that can be used for continuous authentication and liveness detection to detect fake PPG signals without adding other sensing components. Figure 2 presents an overview of the countermeasure (surrounded by dashed lines) in PPG-based authentication. The countermeasure repeats the PPG recording, extracts feature values from the PPG signals, and identifies the measurement sites after the initial authentication. The identification rejects inputs derived from non-genuine measurement sites as fake signals and accepts inputs from genuine sites as genuine signals to repeat the procedure.

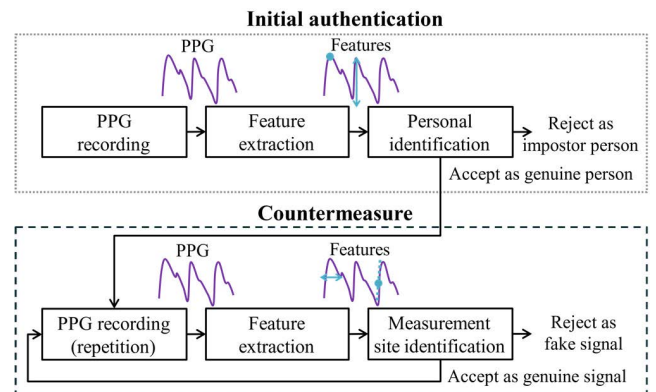


FIGURE 2. Scheme of the proposed countermeasure for PPG-based biometric authentication.

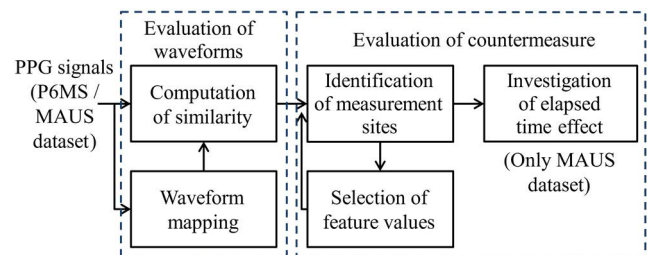


FIGURE 3. Overview of the experimental scheme.

The repetition frequency of the proposed countermeasure is important for continuous authentication in terms of the tradeoff the relationship between the possibility of false rejection and false acceptance [24]. Hernandez-Ortega et al. set the time length of frames for PPG signals recorded by a camera to extract feature values, such as peaks in one period, for continuous authentication in a face recognition [29]. Following the setting, we set the repetition frequency of identification as the countermeasure for every period as a segment in the PPG signals.

## IV. EXPERIMENT

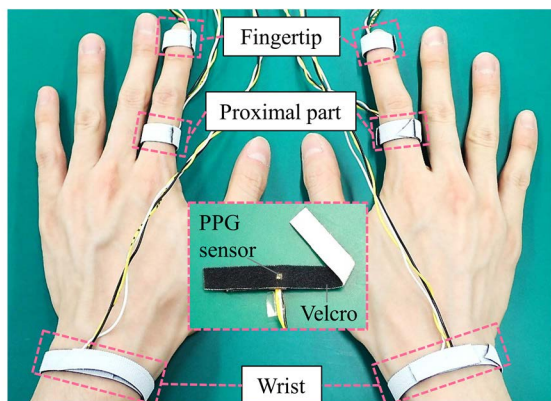
We conducted an experiment to evaluate the proposed countermeasure against PAs on PPG-based authentication. Figure 3 shows an overview of the experimental scheme. Before the evaluation of the countermeasure, we evaluated PPG waveforms by computing the similarity between PPG signals recorded at multiple measurement sites on participants and mapping waveforms using the signals to estimate the original signals. Subsequently, we evaluated the proposed countermeasure by identifying the measurement site by changing the selected feature values and investigating the effect of elapsed time on the countermeasure.

### A. DATASETS

In the experiment, we used two datasets of PPG signals recorded at multiple measurement sites from a total of 34 participants. Table 1 shows a comparison of the datasets.

**TABLE 1.** Comparison of PPG signal datasets used for the experiment.

Dataset	No. of participants (female / male)	Ages	Recording state (duration)	Measurement sites	Sampling rate	LED color (wavelength)
P6MS	12 (1 / 11)	27.3 ± 1.8	Resting (180 s)	Fingertip, proximal part, and wrist (left and right)	1 kHz	Green (570 nm)
MAUS	22 (2 / 20)	23.0 ± 1.7	Resting (180 s) and $n$ -back task (300 s) × 6	Fingertip (non-dominant) Wrist (non-dominant)	256 Hz 100 Hz	Infrared (N.A.) Green (N.A.)

**FIGURE 4.** PPG measurement sites in P6MS dataset.

### 1) P6MS DATASET

Our PPG at six measurement sites (P6MS) dataset included PPG signals recorded at six measurement sites (left and right wrists, proximal parts, and fingertips) on 12 participants (S1, S2, . . . , S12) who did not have any cardiovascular diseases using a developed PPG sensing system. PPG signals were obtained from participants when they rested for 180 s. The sensing system included six PPG sensors consisting of an LED and a PTR (NJL5303R-TE1, New Japan Radio Co., Ltd.). Each output of the PTR was filtered with a low-frequency cutoff of 0.40 Hz and a high-frequency cutoff of 5.0 Hz, amplified with a gain of 47 dB and a sampling rate of 1 kHz with a resolution of 16 bits, and recorded using an analog-digital (AD) converter (USB-6216, National Instruments). The sensors were fastened using Velcro tape to record the PPG signals on the fingertip, proximal part, and wrist of each hand (Fig. 4). Although more candidates are available for PPG measurement sites, we selected six sites as our scope to evaluate the proposed countermeasure using PPG signals recorded on relatively similar and close sites, which might resemble each other in waveform based on the symmetry of the body, blood vessel configuration, and blood circulation. In addition, PPG signals are generally recorded on fingertips in many clinical applications [31], whereas smartwatches record PPG signals on wrists. Moreover, wearable ring-type devices on the proximal part are commercially available [32]. The measurements were approved by the Ethical Committee of the Information Technology R&D Center (2020-B001), Mitsubishi Electric Corporation, Japan.

Informed consent was obtained from the participants before the recording began.

### 2) MAUS DATASET

In addition to P6MS dataset, we used mental workload assessment on  $n$ -back task using wearable sensor (MAUS) dataset [33] in the experiment. It is the only open access dataset that includes PPG signals recorded at two measurement sites (non-dominant wrist and fingertip) on 22 healthy participants. PPG signals were obtained from the participants when they were resting for 300 s and performing  $n$ -back tasks for six trials (Trials 1-6) for 300 s successively with intervals of 120 s. In the  $n$ -back task, participants were required to memorize the last  $n$  numbers of a series of rapidly flashing numbers in succession ( $n = 0, 2, \text{ and } 3$ ). When a number was identical to the  $n$ -th number preceding the stimulus number, participants were required to respond by pressing a button [34]. PPG signals at the fingertip were recorded using a sensor comprising an infrared LED with a sampling rate of 256 Hz with a resolution of 14 bits, and recorded using an AD converter (ProComp Infinity, Thought Technology) [35]. PPG signals at the wrist were recorded using a sensor comprising a green LED with a sampling rate of 100 Hz and recorded using a smartwatch (PixArt PPG Watch) [34], [36]. Both PPG signals were up-sampled at 1 kHz by applying linear interpolation and filtered with a low-frequency cutoff of 0.40 Hz and a high-frequency cutoff of 5.0 Hz to conduct the experiment using the P6MS and MAUS datasets in the same condition. Because the units of PPG signals in the MAUS dataset were not open to the public, before extracting feature values from the signals, we computed the normalized PPG segments as follows:

$$v_{i,\text{norm}}[m] = \frac{v_i[m] - v_{i,\text{min}}}{v_{i,\text{max}} - v_{i,\text{min}}}, \quad (1)$$

where  $i$ ,  $v_i[m]$ ,  $m$ ,  $v_{i,\text{max}}$ , and  $v_{i,\text{min}}$  denote the number of PPG segments,  $i$ -th PPG segment, discrete time, maximum value of  $v_i[m]$ , and minimum value of  $v_i[m]$ , respectively.

## B. EVALUATION OF WAVEFORMS

### 1) COMPUTATION OF SIMILARITY

To evaluate the similarity of the PPG waveforms that may contribute to the capability of the PPG-based authentication, PA, and proposed countermeasure, we computed the Pearson correlation coefficients (CORR) between two PPG signals

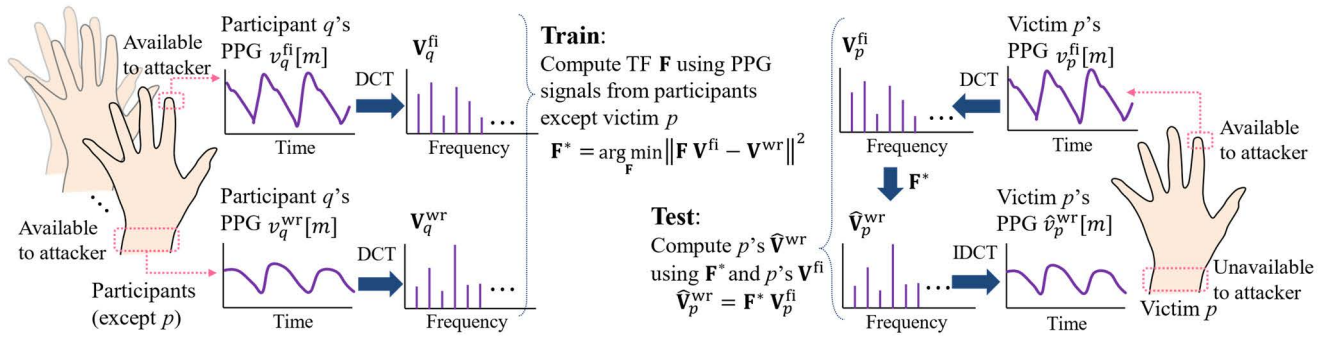


FIGURE 5. Overview of the PPG waveform mapping scheme. An example using the left PPG<sup>fi</sup> to estimate the left PPG<sup>wr</sup> is shown.

because CORR is the most robust metric for measuring similarity in time-series physiological signals [37]. Additionally, the CORR can be used as an evaluation metric to identify a person as genuine in a PPG-based authentication [38]. In the computation, we assumed that PPG signals recorded at the left wrist (PPG<sup>wr</sup>) in the P6MS dataset were used as genuine inputs to the authentication because they could be recorded by commercially available smartwatches, whereas PPG signals recorded at the fingertip (PPG<sup>fi</sup>) and proximal part (PPG<sup>pr</sup>) were used as fake inputs for authentication. We also assumed that the non-dominant left PPG<sup>wr</sup> were genuine inputs in the P6MS dataset because all participants were right-handed. CORR between the  $i$ -th PPG<sup>wr</sup> segment  $v_i^{wr}[m]$  and PPG<sup>fi</sup> segment  $v_i^{fi}[m]$  is computed as follows:

$$CORR_i = \frac{\sum_{m=1}^M (v_i^{wr}[m] - \bar{v}_i^{wr})(v_i^{fi}[m] - \bar{v}_i^{fi})}{\sqrt{\sum_{m=1}^M (v_i^{wr}[m] - \bar{v}_i^{wr})^2} \sqrt{\sum_{m=1}^M (v_i^{fi}[m] - \bar{v}_i^{fi})^2}}, \quad (2)$$

where  $M$ ,  $\bar{v}_i^{wr}$  and  $\bar{v}_i^{fi}$  denote the length of a segment, mean of  $v_i^{wr}[m]$ , and mean of  $v_i^{fi}[m]$ , respectively.

## 2) WAVEFORM MAPPING

We investigated a waveform mapping technique to estimate the (left) PPG<sup>wr</sup> used for the PA in the experiment. There are several approaches related to the estimation of time-series physiological signal waveforms, such as arterial blood pressure (ABP), ECG, EEG, and PPG, from other signals [9], [39]. Some previous studies have proposed methods to estimate signal waveforms such as ABP and ECG from other signals such as PPG using transfer functions (TFs) based on the similarity between the signals and frequency characteristics computed by conventional signal processing techniques such as discrete cosine transforms (DCT) [39], [40]. TFs can be computed using not only one person's signals but also signals gathered from multiple people, except for a victim [9]. Our previous study also proposed a method of estimating PPG waveforms using TF based on the similarity between PPG signals recorded at different sites and frequency characteristics [18].

TABLE 2. Feature values extracted from PPG signals in the experiment. The selected five values for investigation of elapsed time effect based on PIs are shown in bold.

Feature values	Reference
Number of peaks, <b>positive slant</b> , negative slant, and first peak time	[5]
Mean, <b>standard deviation</b> , <b>dynamic time warping distance</b> , maximum value time, minimum value time, maximum value of wavelet coefficients, <b>minimum value of wavelet coefficients</b> , skewness, and kurtosis	[6]
Peak time, <b>dicrotic notch time</b> , and reflection index	[11]
MFCC1, MFCC2, ..., and MFCC24	[41]

In this study, we mapped the PPG signals to other PPG signals using DCT based on previous studies including ours. Figure 5 shows an overview of the mapping, which provides an example of using the left PPG<sup>fi</sup> to estimate the left PPG<sup>wr</sup>. We assumed that an attacker can gather PPG signals recorded at a genuine wrist and another measurement site on multiple people, except a victim, and obtain only the PPG signal recorded at another measurement site on the victim. The attacker obtains DCT coefficients as  $\mathbf{V}_q^{fi} = (\mathbf{V}_{q,1}^{fi} \mathbf{V}_{q,2}^{fi} \dots \mathbf{V}_{q,N}^{fi})$  and  $\mathbf{V}_q^{wr} = (\mathbf{V}_{q,1}^{wr} \mathbf{V}_{q,2}^{wr} \dots \mathbf{V}_{q,N}^{wr})$  by applying DCT to PPG<sup>fi</sup> and PPG<sup>wr</sup> on multiple people except for one person as the victim  $p (\neq q)$ , where  $N$  denotes the total number of segments. The attacker gathers them as  $\mathbf{V}^{fi} = (\mathbf{V}_1^{fi} \mathbf{V}_2^{fi} \dots \mathbf{V}_Q^{fi})$  except  $\mathbf{V}_p^{fi}$  and  $\mathbf{V}^{wr} = (\mathbf{V}_1^{wr} \mathbf{V}_2^{wr} \dots \mathbf{V}_Q^{wr})$  except  $\mathbf{V}_p^{wr}$ , where  $Q$  denotes the number of participants. Subsequently, the attacker computes the TF as a matrix  $\mathbf{F}$  using the least-squares method as follows (**Train** in Fig. 5):

$$\mathbf{F}^* = \underset{\mathbf{F}}{\operatorname{argmin}} \left\| \mathbf{F} \mathbf{V}^{fi} - \mathbf{V}^{wr} \right\|^2, \quad (3)$$

The attacker estimates the victim  $p$ 's DCT coefficients  $\mathbf{V}_p^{wr}$  as  $\hat{\mathbf{V}}_p^{wr}$  using  $\mathbf{V}_p^{fi}$  as follows:

$$\hat{\mathbf{V}}_p^{wr} = \mathbf{F}^* \mathbf{V}_p^{fi}, \quad (4)$$

Finally, the attacker computes  $p$ 's left PPG<sup>wr</sup> as the left PPG<sup>wr</sup>  $\hat{v}_p^{wr}$  by applying inverse DCT (IDCT) to  $\hat{\mathbf{V}}_p^{wr}$

(Test in Fig. 5).  $\hat{V}_p^{wr}$  is used for the comparison of waveforms and evaluation of the countermeasure.

### C. EVALUATION OF COUNTERMEASURE

#### 1) IDENTIFICATION OF MEASUREMENT SITES

We extracted feature values from PPG segments of recorded signals at multiple measurement sites on participants and mapped the signals using the recorded signals, as described in the previous section. Table 2 shows a list of 40 feature values extracted from the segments based on previous studies [5], [6], [11], [41]. They included 24 Mel-frequency cepstral coefficients (MFCC1, . . . , MFCC24): that were often used in audio signal-processing systems [41]. We did not use the maximum and minimum values [6], [11] as the feature values because we applied normalization to PPG segments in MAUS dataset. We conducted  $k$ -fold cross-validation to evaluate and select the feature values for the countermeasure. To use 30 s duration signals for validation, we set  $k = 6$  and 10 when using the P6MS and MAUS datasets, respectively. In the validation, we generated a support vector machine (SVM) classifier, which was successfully applied to several biometric systems including PPG-based authentication [42].

#### 2) SELECTION OF FEATURE VALUES

During the evaluation, we changed the number and combination of feature values to investigate the optimal feature values for the identification of PPG measurement sites as the proposed countermeasure. It is desirable to use fewer feature values in the proposed countermeasure than the values in the initial PPG-based authentication in terms of soft biometrics in continuous authentication. Therefore, we evaluated the feature values by computing the permutation importance (PI) and select them based on the PIs for the countermeasure. The PI was computed by shuffling one column of a dataset of feature values to generate a corrupted dataset and calculating the classification performance using the corrupted dataset. The PI for the feature value  $h$  is defined as follows [43]:

$$PI_h = s - \frac{1}{R} \sum_{r=1}^R s_{r,h}, \quad (5)$$

where  $s$ ,  $h$ ,  $R$ , and  $s_{r,h}$  denote the accuracy, number of feature values, total number of repetitions, and accuracy using the corrupted feature values, respectively.  $s$  is calculated as follows:

$$s = \frac{TP + TN}{TP + FP + TN + FN}, \quad (6)$$

where TP, TN, FP, and FN are defined as true positive, true negative, false positive, and false negative, respectively [44].

#### 3) INVESTIGATION OF ELAPSED TIME EFFECT

We investigated the effect of elapsed time on the countermeasure as the time stability of the measurement site identification in terms of continuous authentication because PPG waveforms gradually change, which may contribute to the capability of the identification. We used the MAUS dataset in

**TABLE 3. Comparison of CORRs between the left PPG<sup>wr</sup> and PPG signals recorded at the other measurement sites using P6MS dataset.**

Measurement site	Original PPG	Mapped PPG
Left fingertip	0.829 ± 0.100	0.874 ± 0.080
Left proximal part	0.835 ± 0.111	0.879 ± 0.073
Right fingertip	0.818 ± 0.116	0.862 ± 0.084
Right proximal part	0.844 ± 0.090	0.863 ± 0.090
Right wrist	0.845 ± 0.118	0.872 ± 0.089

**TABLE 4. Comparison of CORRs between the PPG<sup>wr</sup> and PPG<sup>fi</sup> for each trial using MAUS dataset.**

Trial (task)	Original PPG	Mapped PPG
Resting	0.676 ± 0.132	0.919 ± 0.068
Trial 1 (0-back)	0.700 ± 0.141	0.928 ± 0.072
Trial 2 (2-back)	0.705 ± 0.136	0.920 ± 0.073
Trial 3 (3-back)	0.729 ± 0.121	0.917 ± 0.081
Trial 4 (2-back)	0.724 ± 0.110	0.933 ± 0.055
Trial 5 (3-back)	0.727 ± 0.123	0.917 ± 0.064
Trial 6 (0-back)	0.721 ± 0.115	0.929 ± 0.056

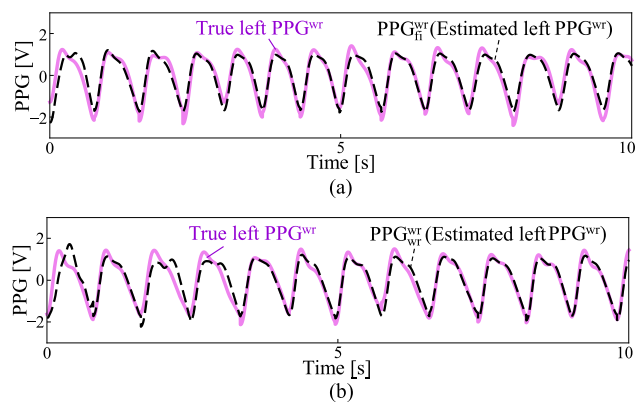


**FIGURE 6. Examples of PPG mapping result using the P6MS dataset. (a) Comparison of left PPG<sup>wr</sup> and left PPG<sup>wr</sup> (participant ID: S12). (b) Comparison of left PPG<sup>wr</sup> and right PPG<sup>wr</sup> (participant ID: S06). The true waveforms (solid lines) and estimated waveforms (dashed lines) by mapping are compared.**

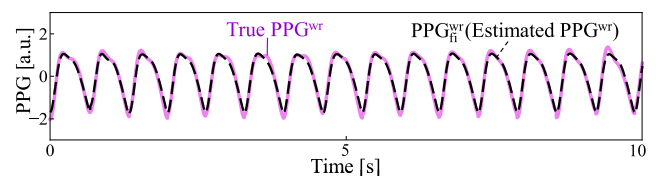


**FIGURE 7. Example of PPG mapping result using the MAUS dataset (participant ID: 012, recording state: resting). The true waveforms (solid lines) and estimated waveforms (dashed lines) by mapping are compared.**

the evaluation because it included PPG signals recorded for a total of 47 min (one resting for 300 s and six  $n$ -back trials for 300 s with six intervals for 120 s), which had a longer duration than the P6MS dataset (one resting for 180 s). We generated an SVM classifier using the top five feature values in the resting data and tested the classifier using the values from trials (Trials 1-6) to compute accuracy in each Trial. The feature values were selected for evaluation by computing

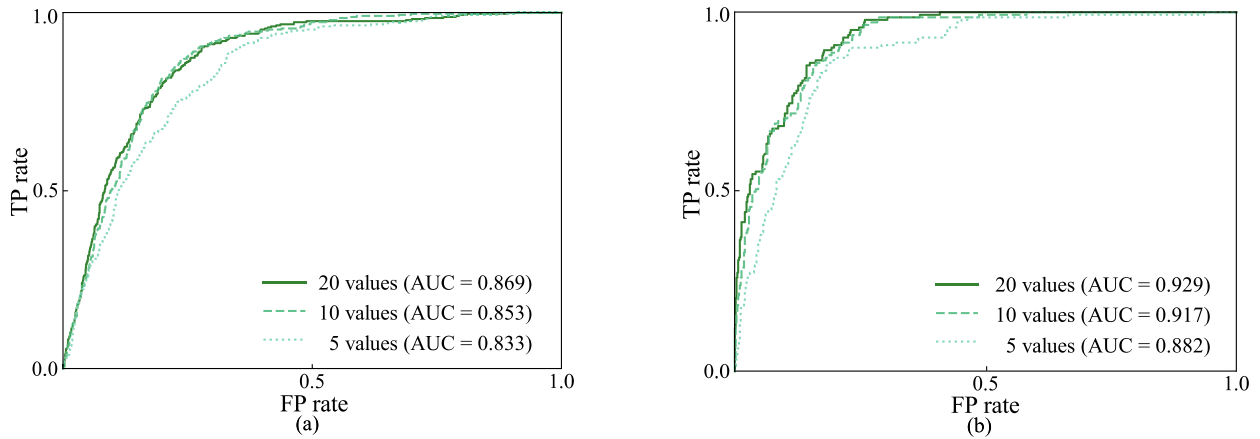


**FIGURE 8.** Comparison of ROC curves by changing the number of feature values when using the P6MS dataset. (a) Original PPG signals. (b) Mapped PPG signals.

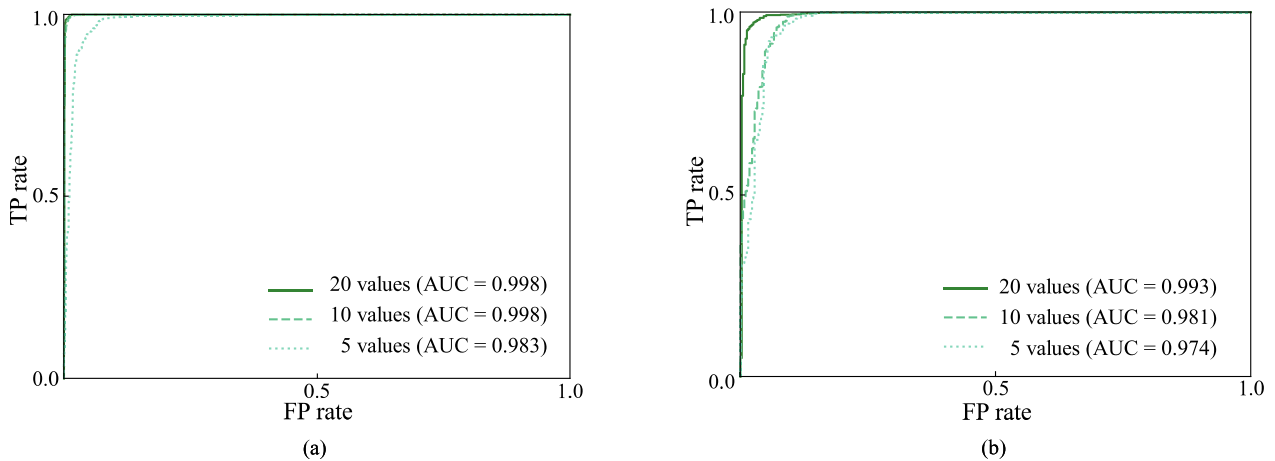


**FIGURE 9.** Comparison of ROC curves by changing the number of feature values when using the MAUS dataset. (a) Original PPG signals. (b) Mapped PPG signals.

the PI of each feature value in the previous evaluation of identification using all feature values.

**V. RESULTS AND DISCUSSION**

**A. EVALUATION OF WAVEFORMS**

Tables 3 and 4 list the CORRs between the original PPG signals using the P6MS and MAUS datasets, respectively. All CORRs under the “Original PPG” in Table 3 were larger than 0.800. All CORRs under “Original PPG” in Table 4 were larger than 0.700 except for resting condition. Generally, if  $0.700 < |CORR| < 0.900$  and  $0.900 < |CORR| < 1.000$ , the CORRs indicate high correlation and very high correlation, respectively [45]. In addition, if PPG signals are recorded for a long time at the same measurement sites on the same person, CORRs between the PPG signals satisfy  $CORR > 0.800$  in many conditions [38]. Therefore, the CORRs suggested that the PPG signals recorded at the other measurement sites might be used as fake inputs for PPG-based authentication because of their similarity. To compare the CORRs under “Original PPG” in each

dataset, as shown in Tables 3 and 4, we conducted an analysis of variance (ANOVA) after establishing the homogeneity of variance among the CORRs. The ANOVA results indicated no significant differences between the CORRs in the measurement sites in the P6MS or in the trials in the MAUS dataset.

Tables 3 and 4 also show the CORRs between the PPG<sup>WT</sup> and mapped signals to estimate PPG<sup>WT</sup> using the P6MS and MAUS datasets, respectively. All CORRs under “Mapped PPG” in Table 3 were larger than 0.800 and CORRs under “Original PPG.” All CORRs under “Original PPG” in Table 4 were larger than 0.900 and CORRs under “Original PPG.” Figure 6(a) and (b) show an example of the PPG waveform mapping results using the P6MS dataset. Figure 7 shows an example of the PPG waveform mapping results obtained using the MAUS dataset. Therefore, the results suggested that our PPG mapping method could estimate PPG<sup>WT</sup> using PPG<sup>fi</sup> or PPG<sup>pf</sup> in both datasets with high accuracy, which might contribute to the PA. To compare the CORRs of “Mapped PPG” in each dataset, as shown in Tables 3 and 4,

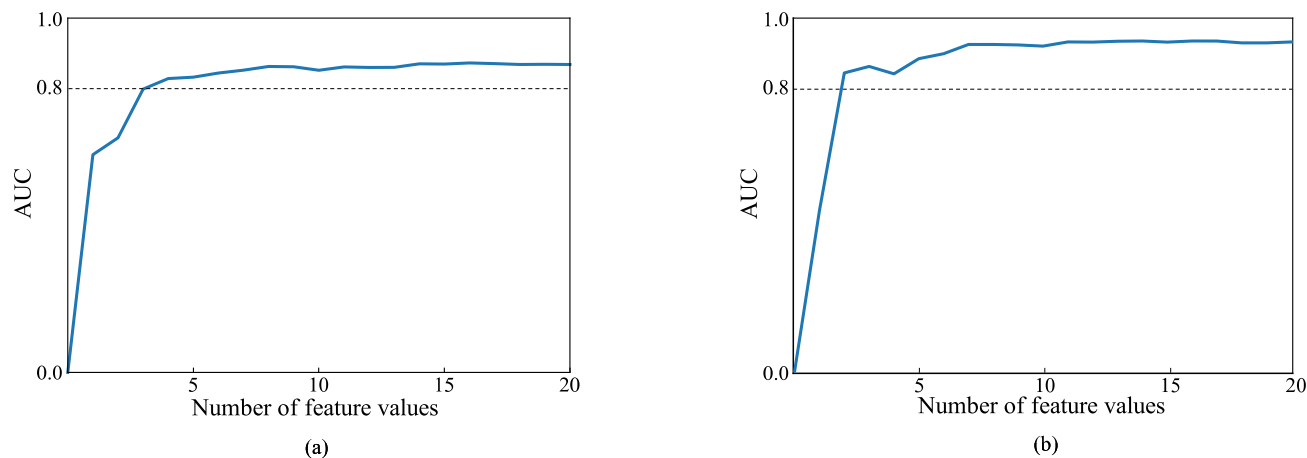


FIGURE 10. Relationship between AUC and number of feature values when using the P6MS dataset. (a) Original PPG signals. (b) Mapped PPG signals.

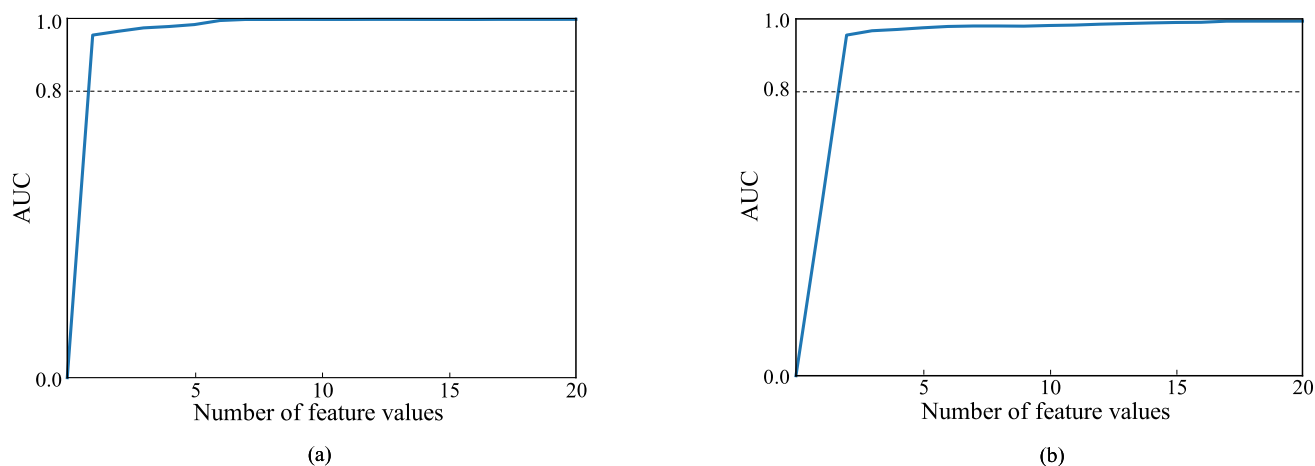


FIGURE 11. Relationship between AUC and number of feature values when using the MAUS dataset. (a) Original PPG signals. (b) Mapped PPG signals.

we conducted ANOVA using the same procedure as in the previous paragraph, and the results indicated no significant differences between CORRs in the measurement sites in the P6MS dataset or in the trials in the MAUS dataset.

**B. EVALUATION OF COUNTERMEASURE**

**1) EVALUATION OF MEASUREMENT SITE IDENTIFICATION**

Figures 8 and 9 show the receiver operating characteristic (ROC) curves of PPG measurement site identification as the proposed countermeasure against the PA in one validation using 5, 10, and 20 feature values extracted from PPG signals in the P6MS and MAUS datasets, respectively. Figures 10 and 11 show the area under the curve (AUC) using 1-20 values for validation in the P6MS and MAUS datasets, respectively. As shown in Figs. 8-11, the AUC converged when more than five values were used. Zhu et al. defined a good classifier as one classifier that had an ROC curve with an  $AUC \geq 0.800$  [44]. Therefore, the result suggested that the identification as the countermeasure operated successfully using at most five feature values for the two datasets,

TABLE 5. Identification accuracy of  $PPG^{wr}$  and  $PPG^{fi}$  for the investigation of elapsed time effect on the countermeasure.

Trial (task)	Original PPG	Mapped PPG
Trial 1 (0-back)	0.966	0.909
Trial 2 (2-back)	0.962	0.928
Trial 3 (3-back)	0.944	0.907
Trial 4 (2-back)	0.951	0.941
Trial 5 (3-back)	0.952	0.953
Trial 6 (0-back)	0.952	0.945

regardless of the presence or absence of waveform mapping. When five feature values were used in the P6MS dataset, the identification accuracies were 0.827 and 0.845 for the original and mapped PPG signals, respectively. When using five values in the MAUS dataset, the accuracies were 0.946 and 0.956 for the original and mapped PPG signals, respectively. The countermeasures required fewer feature values than typical PPG-based authentication with 15-24 values [41], [42]. In addition, the number of values satisfied the condition in the



previous study, which used only nine PPG feature values for continuous authentication in a face-recognition system [29]. The results suggested that at most, five PPG feature values are not sufficient as hard biometrics for typical authentication; however, they can be used as soft biometrics for continuous authentication.

Table 2 shows the top five feature values selected by computing and comparing the PIs for the proposed countermeasures in bold. They did not include any MFCCs computed through multiple signal processing methods, such as the Fourier transform, which reflected the personal distinctiveness of PPG frequency characteristics. Meanwhile, our previous study evaluated the feature values that contributed to the initial PPG-based authentication and PA by computing and comparing PIs, which demonstrated the effectiveness of MFCCs in the initial authentication against the PA [46]. Therefore, the result suggested that the feature values as soft biometrics contributing to the proposed countermeasure might be different from the values as the personal distinctiveness contributing to the initial authentication.

## 2) EVALUATION OF ELAPSED TIME EFFECT

Table 5 shows all identification accuracies using five feature values shown in bold in Table 2 from PPG signals at rest for the SVM classifier, and the values from PPG signals in performing  $n$ -back tasks for inputs to the classifier using the MAUS dataset to evaluate the time stability of the PPG measurement site identification. As shown under “Original PPG” in Table 5, the identification accuracy for  $PPG^{wr}$  and  $PPG^{fi}$  had a decreasing tendency as the recording progressed, which might be because PPG waveforms gradually changed over time. Although the identification accuracy for  $PPG^{wr}$  and mapped signals (under “Mapped PPG”) were smaller than  $PPG^{wr}$  and  $PPG^{fi}$  (under “Original PPG”) except for Trial 5; the accuracies in all trials were higher than 0.900 regardless of the elapsed time. The result indicated that the identification of PPG measurement sites as the proposed countermeasure against the PA operated successfully with or without  $n$ -back tasks during PPG measurement. It also suggested that the countermeasure might operate successfully in a practical scenario such as wearing a smartwatch during other tasks at a desk than  $n$ -back tasks for the same duration as the MAUS dataset (47 min).

## C. COMPARISON OF DATASETS

By comparing the capability of the countermeasures, as shown in Figs. 8-11, the identification of PPG measurement sites was more successful for the MAUS dataset than for the P6MS dataset. The difference might be derived from the number of measurement sites and the PPG sensors used for each dataset. PPG signals in the P6MS dataset were recorded using the same specification sensors for six measurement sites, whereas PPG signals in the MAUS dataset were recorded using different specification sensors for the fingertip and wrist. Generally, longer-wavelength light from infrared LED penetrates deeply into the skin, whereas

shorter-wavelength light from the green LED does not, which contributes to the difference in PPG waveforms [23]. As shown under “Original PPG” in Tables 3 and 4, CORRs as the similarity between  $PPG^{wr}$  and  $PPG^{fi}$  in the MAUS dataset were smaller than those between  $PPG^{wr}$  and other original PPG signals. Therefore, the identification of PPG measurement sites as a countermeasure might be more effective for the MAUS dataset than for the P6MS dataset.

However, by comparing the CORRs in “Mapped PPG” in Tables 3 and 4, the results indicate that the mapping achieved a better capability for the MAUS than the P6MS dataset. We applied linear interpolation and a band-pass filter to the signals in the MAUS dataset to conduct the experiment under the same conditions for both datasets, which might have resulted in a decrease in the personal distinctiveness of the signals in the MAUS dataset to generate all similar signals.

## D. LIMITATIONS

Under limited experimental conditions, we evaluated the identification of PPG measurement sites as the proposed countermeasure against the PA on PPG-based authentication. We must address the following two limitations of the study:

### 1) MEASUREMENT CONDITIONS

In our future studies, we must conduct an experiment using PPG signals recorded at various measurement sites on more participants in various age ranges and health conditions in other recording states. In the evaluation, we used PPG signals recorded at only two or six measurement sites on 20-30 years old healthy participants in the two datasets, whereas other several sites could be utilized, such as the face, earlobe, and toe. The differences in PPG waveforms derived from ages and cardiovascular diseases and the difficulty in extracting segments and feature values from the waveforms may affect the performance of the measurement site identification. In addition, other recording states such as walking may add motion artifacts to the PPG waveforms and decrease the accuracy of identification. However, we expect that the identification may be successful for PPG signals recorded at distant sites from the wrist because PPG waveforms recorded at closer sites tend to be more similar to each other. For example, the finger and wrist, and the earlobe and forehead provide more similar PPG waveforms based on the blood vessel configuration and blood circulation [11]. In addition, Li et al. evaluated the feasibility of PA using PPG at the face using a camera, and concluded that the difficulty of PA is due to the camera specification such as frame rate when generating fake signals [16]. Therefore, the proposed countermeasure may identify PPG signals on the face using a camera with a low frame rate and mapped signals using the PPG signals on the face.

### 2) WAVEFORM MAPPING TECHNIQUE

Other waveform mapping techniques should be applied to PPG signals to evaluate the proposed countermeasure in our future studies. We applied only one technique using the TF computed using PPG signals from participants based on the

frequency characteristics, although the result exhibited the effectiveness of estimating PPG<sup>WT</sup>. Techniques for mapping based on deep learning techniques, such as GAN [16], are available, which might generate fake signals that are more similar to genuine PPG signals compared with our technique.

## VI. CONCLUSION

In this paper, we proposed a countermeasure against PAs on PPG-based biometric authentication. The countermeasure detects fake PPG signals by identifying PPG measurement sites on the body based on the difference between PPG waveforms recorded at genuine measurement and non-genuine sites without adding other sensing components. We evaluated the countermeasure using two datasets, including PPG signals recorded at multiple measurement sites for 34 participants. We compared PPG<sup>WT</sup> and PPG signals recorded at other measurement sites and mapped signals based on the frequency characteristics to estimate PPG<sup>WT</sup> used for authentication by computing CORRs as the similarity index between the signals. The result indicated the similarity between the PPG signals PPG<sup>WT</sup> and other PPG signals as the CORRs between them satisfied  $\text{CORR} > 0.700$  in most of the trials in both datasets. Subsequently, we extracted the feature values from the PPG signals and generated an SVM classifier to identify the measurement sites against the PA. The results indicated the effectiveness of PPG measurement site identification for both datasets, regardless of the presence or absence of waveform mapping with  $\text{AUC} > 0.800$ . In addition, the investigation results of the elapsed time effect on the countermeasure indicated the time stability of the identification with an accuracy of more than 90%. Our future research will include evaluation using PPG signals recorded on more diverse participants in other recording states and other waveform mapping techniques.

## REFERENCES

- [1] G.-J. Jong, A. Aripriharta, and G.-J. Hornig, "The PPG physiological signal for heart rate variability analysis," *Wireless Pers. Commun.*, vol. 97, no. 4, pp. 5229–5276, Aug. 2017. [Online]. Available: <https://link.springer.com/article/10.1007/s11277-017-4777-z#citeas> and <https://www.researchgate.net/profile/Aripriharta-Aripriharta>
- [2] Y. Contoyiannis, F. K. Diakonos, M. Kampitakis, and S. M. Potirakis, "Can high-frequency ECG fluctuations differentiate between healthy and myocardial infarction cases?" *Biomed. Eng. Adv.*, vol. 2, Dec. 2021, Art. no. 100011.
- [3] Y. Sun and N. Thakor, "Photoplethysmography revisited: From contact to noncontact, from point to imaging," *IEEE Trans. Biomed. Eng.*, vol. 63, no. 3, pp. 463–477, Mar. 2015.
- [4] M. A. F. Pimentel, A. E. W. Johnson, P. H. Charlton, D. Birrenkott, P. J. Watkinson, L. Tarassenko, and D. A. Clifton, "Toward a robust estimation of respiratory rate from pulse oximeters," *IEEE Trans. Biomed. Eng.*, vol. 64, no. 8, pp. 1914–1923, Nov. 2016.
- [5] Y. Y. Gu, Y. Zhang, and Y. T. Zhang, "A novel biometric approach in human verification by photoplethysmographic signals," in *Proc. 4th Int. IEEE EMBS Special Topic Conf. Inf. Technol. Appl. Biomed. (ITAB)*, Birmingham, U.K., Apr. 2003, pp. 13–14.
- [6] V. Jindal, J. Birjandtalab, M. B. Pouyan, and M. Nourani, "An adaptive deep learning approach for PPG-based identification," in *Proc. 38th Annu. Int. Conf. IEEE Eng. Med. Biol. Soc. (EMBC)*, Orlando, FL, USA, Aug. 2016, pp. 6401–6404.
- [7] T. Zhao, Y. Wang, J. Liu, J. Cheng, Y. Chen, and J. Yu, "Robust continuous authentication using cardiac biometrics from wrist-worn wearables," *IEEE Internet Things J.*, vol. 9, no. 12, pp. 9542–9556, Jun. 2022.
- [8] S. Eberz, N. Paoletti, M. Roeschlin, A. Patané, M. Kwiatkowska, and I. Martinovic, "Broken hearted: How to attack ECG biometrics," in *Proc. Netw. Distrib. Syst. Secur. Symp.*, San Diego, CA, USA, 2017, pp. 1–15.
- [9] D. Shukla, P. P. Kundu, R. Malapati, S. Poudel, Z. Jin, and V. V. Phoha, "Thinking unveiled: An inference and correlation model to attack EEG biometrics," *Digit. Threats, Res. Pract.*, vol. 1, no. 2, pp. 1–29, Jun. 2020.
- [10] R. M. Seepers, W. Wang, G. de Haan, I. Sourdis, and C. Strydis, "Attacks on heartbeat-based security using remote photoplethysmography," *IEEE J. Biomed. Health Informat.*, vol. 22, no. 3, pp. 714–721, May 2018.
- [11] V. Hartmann, H. Liu, F. Chen, Q. Qiu, S. Hughes, and D. Zheng, "Quantitative comparison of photoplethysmographic waveform characteristics: Effect of measurement site," *Frontiers Physiol.*, vol. 10, Mar. 2019, Art. no. 198.
- [12] Y. Maeda, M. Sekine, and T. Tamura, "Relationship between measurement site and motion artifacts in wearable reflected photoplethysmography," *J. Med. Syst.*, vol. 35, no. 5, pp. 969–976, May 2011.
- [13] K. A. Reddy, B. George, and V. J. Kumar, "Use of Fourier series analysis for motion artifact reduction and data compression of photoplethysmographic signals," *IEEE Trans. Instrum. Meas.*, vol. 58, no. 5, pp. 1706–1711, May 2009.
- [14] A. Fujii, K. Murao, and N. Matsuhisa, "disp2ppg: Pulse wave generation to PPG sensor using display," in *Proc. Int. Symp. Wearable Comput.*, USA, Sep. 2021, pp. 119–123. [Online]. Available: <https://www.iswc.net/iswc21/>
- [15] Y. Akimoto and K. Murao, "Design and implementation of an input interface for wearable devices using pulse wave control by compressing the upper arm," in *Proc. Augmented Hum. Conf.*, Rovaniemi, Finland, Feb. 2021, pp. 280–282.
- [16] L. Li, C. Chen, L. Pan, J. Zhang, and Y. Xiang, "Video is all you need: Attacking PPG-based biometric authentication," 2022, [arXiv:2203.00928](https://arxiv.org/abs/2203.00928).
- [17] S. Hinatsu, D. Suzuki, H. Ishizuka, S. Ikeda, and O. Oshiro, "Basic study on presentation attacks against biometric authentication using photoplethysmogram," *Adv. Biomed. Eng.*, vol. 10, pp. 101–112, Jul. 2021.
- [18] S. Hinatsu, D. Suzuki, H. Ishizuka, S. Ikeda, and O. Oshiro, "Attack on PPG biometrics: Presentation attack by stealth recording and waveform estimation," in *Proc. 43rd Annu. Int. Conf. IEEE Eng. Med. Biol. Soc. (EMBC)*, Guadalajara, Mexico, Nov. 2021, pp. 64–67.
- [19] T. Herzog and A. Uhl, "Analysing a vein liveness detection scheme," in *Proc. 8th Int. Workshop Biometrics Forensics (IWBF)*, Porto, Portugal, Apr. 2020, pp. 1–6.
- [20] S. A. C. Schuckers, "Spoofing and anti-spoofing measures," *Inf. Secur. Tech. Rep.*, vol. 7, no. 4, pp. 56–62, Dec. 2002.
- [21] K. Kavita, G. S. Walia, and R. Rohilla, "A contemporary survey of unimodal liveness detection techniques: Challenges & opportunities," in *Proc. 3rd Int. Conf. Intell. Sustain. Syst. (ICISS)*, Thoothukudi, India, Dec. 2020, pp. 848–855.
- [22] J. Spooren, D. Preuveneers, and W. Joosen, "PPG2Live: Using dual PPG for active authentication and liveness detection," in *Proc. Int. Conf. Biometrics (ICB)*, Crete, Greece, Jun. 2019, pp. 1–6.
- [23] Y. Maeda, M. Sekine, and T. Tamura, "The advantages of wearable green reflected photoplethysmography," *J. Med. Syst.*, vol. 35, no. 5, pp. 829–834, May 2011.
- [24] K. Niinuma, U. Park, and A. K. Jain, "Soft biometric traits for continuous user authentication," *IEEE Trans. Inf. Forensics Security*, vol. 5, no. 4, pp. 771–780, Dec. 2010.
- [25] A. Dantcheva, P. Elia, and A. Ross, "What else does your biometric data reveal? A survey on soft biometrics," *IEEE Trans. Inf. Forensics Security*, vol. 11, no. 3, pp. 441–467, Mar. 2015.
- [26] S. S. Gornale, "Fingerprint based gender classification for biometric security: A state-of-the-art technique," *Amer. Int. J. Res. Sci. Technol. Eng. Math.*, vol. 9, no. 1, pp. 39–49, Feb. 2015.
- [27] R. Zewail, A. Elsaifi, M. Saeb, and N. Hamdy, "Soft and hard biometrics fusion for improved identity verification," in *Proc. 47th Midwest Symp. Circuits Syst. (MWSCAS)*, Hiroshima, Japan, Jul. 2004, pp. 225–228.
- [28] S. Vhaduri and C. Poellabauer, "Multi-modal biometric-based implicit authentication of wearable device users," *IEEE Trans. Inf. Forensics Security*, vol. 14, no. 12, pp. 3116–3125, Dec. 2019.
- [29] J. Hernandez-Ortega, J. Fierrez, E. Gonzalez-Sosa, and A. Morales, "Continuous presentation attack detection in face biometrics based on heart rate," in *Video Analytics. Face and Facial Expression Recognition*. Beijing, China: Springer, Aug. 2018, pp. 72–86. [Online]. Available: [https://link.springer.com/chapter/10.1007/978-3-030-12177-8\\_7](https://link.springer.com/chapter/10.1007/978-3-030-12177-8_7)
- [30] G. N. K. Reddy, M. S. Manikandan, and N. V. L. N. Murty, "On-device integrated PPG quality assessment and sensor disconnection/saturation detection system for IoT health monitoring," *IEEE Trans. Instrum. Meas.*, vol. 69, no. 9, pp. 6351–6361, Sep. 2020.

- [31] M. Hosanee, G. Chan, K. Welykholowa, R. Cooper, P. A. Kyriacou, D. Zheng, J. Allen, D. Abbott, C. Menon, N. H. Lovell, N. Howard, W.-S. Chan, K. Lim, R. Fletcher, R. Ward, and M. Elgendi, "Cuffless single-site photoplethysmography for blood pressure monitoring," *J. Clin. Med.*, vol. 9, no. 3, p. 723, Mar. 2020.
- [32] A. Maijala, H. Kinnunen, H. Koskimäki, T. Jämsä, and M. Kangas, "Nocturnal finger skin temperature in menstrual cycle tracking: Ambulatory pilot study using a wearable Oura ring," *BMC Women's Health*, vol. 19, no. 1, pp. 1–10, Nov. 2019.
- [33] W.-K. Beh, Y.-H. Wu, and A.-Y. Wu, "MAUS: A dataset for mental workload assessment on N-back task using wearable sensor," IEEE Dataport, 2021. [Online]. Available: <https://ieee-dataport.org/open-access/maus-dataset-mental-workload-assessment-n-backtask-using-wearable-sensor>, doi: 10.21227/q4td-yd35.
- [34] W.-K. Beh, Y.-H. Wu, and A.-Y. Wu, "MAUS: A dataset for mental workload assessment on N-back task using wearable sensor," 2021, *arXiv:2111.02561*.
- [35] T. Aydemir, M. Şahin, and O. Aydemir, "Sequential forward mother wavelet selection method for mental workload assessment on N-back task using photoplethysmography signals," *Infr. Phys. Technol.*, vol. 119, Dec. 2021, Art. no. 103966.
- [36] W.-K. Beh, Y.-H. Wu, and A.-Y. Wu, "Robust PPG-based mental workload assessment system using wearable devices," *IEEE J. Biomed. Health Informat.*, early access, Dec. 28, 2022, doi: 10.1109/JBHI.2021.3138639.
- [37] A. Kianimajd, M. G. Ruano, P. Carvalho, J. Henriques, T. Rocha, S. Paredes, and A. E. Ruano, "Comparison of different methods of measuring similarity in physiologic time series," *IFAC-PapersOnLine*, vol. 50, no. 1, pp. 11005–11010, Jul. 2017.
- [38] O. R. Patil, W. Wang, Y. Gao, W. Xu, and Z. Jin, "A non-contact PPG biometric system based on deep neural network," in *Proc. IEEE 9th Int. Conf. Biometrics Theory, Appl. Syst. (BTAS)*, Redondo Beach, CA, USA, Oct. 2018, pp. 1–7.
- [39] Q. Zhu, X. Tian, C.-W. Wong, and M. Wu, "ECG reconstruction via PPG: A pilot study," in *Proc. IEEE EMBS Int. Conf. Biomed. Health Informat. (BHI)*, Chicago, IL, USA, May 2019, pp. 1–4.
- [40] A. Dash, N. Ghosh, A. Patra, and A. D. Choudhury, "Estimation of arterial blood pressure waveform from photoplethysmogram signal using linear transfer function approach," in *Proc. 42nd Annu. Int. Conf. IEEE Eng. Med. Biol. Soc. (EMBC)*, Montreal, QC, Canada, Jul. 2020, pp. 2691–2694.
- [41] A. I. Siam, A. A. Elazm, N. A. El-Bahnasawy, G. M. E. Banby, and F. E. A. El-Samie, "PPG-based human identification using Mel-frequency cepstral coefficients and neural networks," *Multimedia Tools Appl.*, vol. 80, pp. 1–19, Apr. 2021. [Online]. Available: <https://link.springer.com/article/10.1007/s11042-021-10781-8>
- [42] G. Lovisotto, H. Turner, S. Eberz, and I. Martinovic, "Seeing red: PPG biometrics using smartphone cameras," in *Proc. IEEE/CVF Conf. Comput. Vis. Pattern Recognit. Workshops (CVPRW)*, Seattle, WA, USA, Jun. 2020, pp. 3565–3574.
- [43] G. Zhang, M. Wang, and K. Liu, "Deep neural networks for global wildfire susceptibility modelling," *Ecol. Indicators*, vol. 127, Aug. 2021, Art. no. 107735.
- [44] W. Zhu, N. Zeng, and N. Wang, "Sensitivity, specificity, accuracy, associated confidence interval and roc analysis with practical SAS implementations," *NESUG Health Care Life Sci.*, vol. 19, pp. 1–9, Nov. 2010.
- [45] M. M. Mukaka, "A guide to appropriate use of correlation coefficient in medical research," *Malawi Med. J.*, vol. 24, no. 3, pp. 69–71, Sep. 2012.
- [46] S. Hinatsu, D. Suzuki, H. Ishizuka, S. Ikeda, and O. Oshiro, "Evaluation of PPG feature values toward biometric authentication against presentation attacks," *IEEE Access*, vol. 10, pp. 41352–41361, 2022.



**SHUN HINATSU** received the M.S. degree from Osaka University, Japan, in 2017, where he is currently pursuing the Ph.D. degree with the Graduate School of Engineering Science. In 2017, he joined Mitsubishi Electric Corporation, Japan. His research interests include biomedical instrumentation and biometric authentication.



**NORI MATSUDA** received the Ph.D. degree from Shizuoka University, Japan, in 2022. In 1997, he joined Mitsubishi Electric Corporation, Japan. His research interests include pairing cryptography, privacy protection, and cryptographic protocols. He is a member of the Institute of Electronics, Information and Communication Engineers.



**HIROKI ISHIZUKA** received the Ph.D. degree from Keio University, in 2016. He was an Assistant Professor at the Department of Engineering, Kagawa University, from 2016 to 2019. He is currently an Assistant Professor with the Graduate School of Engineering Science, Osaka University. His research interests include haptics and soft robotics. He is a member of the Society of Instrument and Control Engineers, the Japan Society of Mechanical Engineers, and the Virtual Reality Society of Japan.



**SEI IKEDA** (Member, IEEE) received the Ph.D. degree from the Nara Institute of Science and Technology, Ikoma, Japan, in 2006. He has worked as an Assistant Professor at the Graduate School of Information Science, Nara Institute of Science and Technology, until 2011, and the Graduate School of Engineering Science, Osaka University, until 2015. He was also a Visiting Researcher at the University of Oulu, Finland, from 2010 to 2011. He was a Lecturer with the College of Information Science and Engineering, Ritsumeikan University, from 2015 to 2019. Since 2019, he has been an Associate Professor with the Graduate School of Engineering Science, Osaka University. His research interests include human–computer interaction, mixed reality, and computer vision. He is a member of the Institute of Electronics, Information and Communication Engineers, the Virtual Reality Society of Japan, and ACM.



**OSAMU OSHIRO** received the Ph.D. degree from Osaka University, Toyonaka, Japan, in 1990. He was a Research Engineer with Sumitomo Metal Industries, from 1990 to 1993, and an Assistant/Associate Professor at the Nara Institute of Science and Technology, from 1993 to 2003. Since 2003, he has been a Professor with the Graduate School of Engineering Science, Osaka University. His research interests include biomedical engineering, medical imaging, and biomedical signal processing. He is a member of Japanese Society for Medical and Biological Engineering, the Institute of Electronics, Information and Communication Engineers, the Institute of Systems, Control and Information Engineers, and the Virtual Reality Society of Japan.

...